

Highly Efficient and Stable Narrow-Band Red Phosphor $\text{Cs}_2\text{SiF}_6:\text{Mn}^{4+}$ for High-Power Warm White LED Applications

Enhai Song,[†] Yayun Zhou,[†] Xiao-Bao Yang,^{*,‡} Zifeng Liao,[§] Weiren Zhao,[§] Tingting Deng,[†] Lingyan Wang,[†] Yanyan Ma,[†] Shi Ye,[†] and Qinyuan Zhang^{*,†}

[†]State Key Laboratory of Luminescent Materials and Devices and Institute of Optical Communication Materials, South China University of Technology, Guangzhou 510641, China

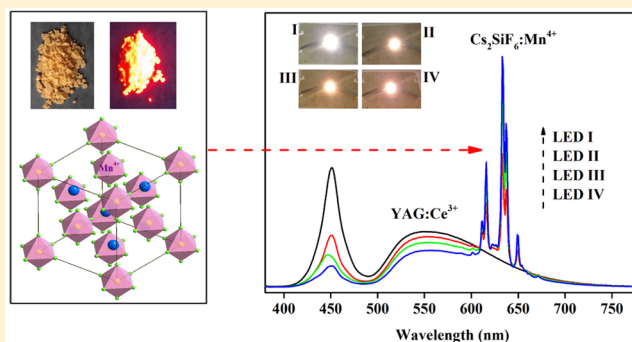
[‡]Department of Physics, South China University of Technology, Guangzhou 510641, China

[§]School of Physics & Optoelectronic Engineering, Guangdong University of Technology, Guangzhou 510006, China

Supporting Information

ABSTRACT: Due to the unique narrow-band red emission and broadband blue light excitation, as well as milder synthesis conditions, Mn^{4+} ion activated fluoride red phosphors show great promise for white light emitting diode (W-LED) applications. However, as the Mn^{4+} emission belongs to a spin-forbidden transition (${}^2\text{E}_g \rightarrow {}^4\text{A}_2$), it is a fundamental challenge to synthesize these phosphors with a high external quantum efficiency (EQE) above 60%. Herein, a highly efficient and thermally stable red fluoride phosphor, $\text{Cs}_2\text{SiF}_6:\text{Mn}^{4+}$, with a high internal quantum efficiency (IQE) of 89% and ultrahigh EQE of 71% is demonstrated. Furthermore, nearly 95% of the room-temperature IQE and EQE are maintained at 150 °C. The static and dynamic spectral measurements, as well as density functional theory (DFT) calculations, show that the excellent performance of $\text{Cs}_2\text{SiF}_6:\text{Mn}^{4+}$ is due to the Mn^{4+} ions being evenly distributed in the host lattice Cs_2SiF_6 . By employing $\text{Cs}_2\text{SiF}_6:\text{Mn}^{4+}$ as a red light component, stable 10 W high-power warm W-LEDs with a luminous efficiency of ~ 110 lm/W could be obtained. These findings indicate that red phosphor $\text{Cs}_2\text{SiF}_6:\text{Mn}^{4+}$ may be a highly suitable candidate for fabricating high-performance high-power warm white LEDs.

KEYWORDS: stable, narrow-band, Mn^{4+} , red phosphor, ultrahigh quantum efficiency, warm white LED



White light emitting diodes (W-LEDs) have been widely applied in various fields, due to their high efficiency, long lifetime, low energy consumption, and environmental friendliness.^{1–6} However, the mainstream and commercialized W-LEDs based on the combination of a blue InGaN chip and yellow phosphor $\text{Y}_3(\text{Al,Ga})_5\text{O}_{12}:\text{Ce}^{3+}$ ($\text{YAG}:\text{Ce}^{3+}$) suffer from low color rendering index (CRI, $R_a < 80$) and high correlated color temperature (CCT > 4500 K) and are not used in indoor lighting, because of the notoriously deficient red emission from yellow phosphor $\text{YAG}:\text{Ce}^{3+}$.^{7–11} To solve this problem, nitride phosphors such as $(\text{Ca,Sr})\text{AlSiN}_3:\text{Eu}^{2+}$ and $\text{Sr}_2\text{Si}_3\text{N}_8:\text{Eu}^{2+}$ are usually used as red light component to add into the W-LEDs due to their high luminescence efficiencies and good thermal stability.^{12–15} However, the excessive broad absorption (~ 200 – 600 nm) and longer emission wavelength (> 650 nm) of these phosphors significantly lower the luminous efficacy of the devices.^{2–4} Furthermore, the synthesis conditions for the nitride phosphors are usually rather harsh, leading to high cost.^{9,16–19}

In contrast, transition metal Mn^{4+} activated fluoride phosphors possess narrow-band red emission around ~ 630

nm and broad excitation band at ~ 460 nm (with a bandwidth of ~ 50 nm), as well as milder synthesis conditions, showing more promise for warm W-LED applications.²⁰ For these characteristics, considerable attention has been focused on this field and various Mn^{4+} -doped fluoride red phosphors such as $\text{A}_2\text{BF}_6:\text{Mn}^{4+}$ ($\text{A} = \text{NH}_4, \text{Na}, \text{K}, \text{Rb}, \text{Cs}$; $\text{A}_2 = \text{Ba}, \text{Zn}$; $\text{B} = \text{Si}, \text{Ge}, \text{Ti}, \text{Zr}$) and $\text{H}_3\text{XF}_6:\text{Mn}^{4+}$ ($\text{H} = \text{Li}, \text{Na}, \text{K}$; $\text{X} = \text{Al}, \text{Ga}$) have been developed.^{8,21–33} By using a suitable synthesis route, nearly a 100% high internal quantum efficiency (IQE) has been achieved in fluoride phosphor $\text{K}_2\text{TiF}_6:\text{Mn}^{4+}$.² However, since the Mn^{4+} emission belongs to a spin-forbidden transition (${}^2\text{E}_g \rightarrow {}^4\text{A}_2$), it is still a fundamental challenge to synthesize these Mn^{4+} -related fluoride phosphors with external quantum efficiency (EQE) higher than 60%, which is crucial for practical applications.^{2,31,34} The ultrahigh IQE value and relatively low EQE in these Mn^{4+} -doped fluoride are due to the lower absorption efficiency (AE) of Mn^{4+} (usually, $\text{AE} < 60\%$). Increasing the dopant level can effectively improve the AE

Received: July 30, 2017

Published: September 15, 2017

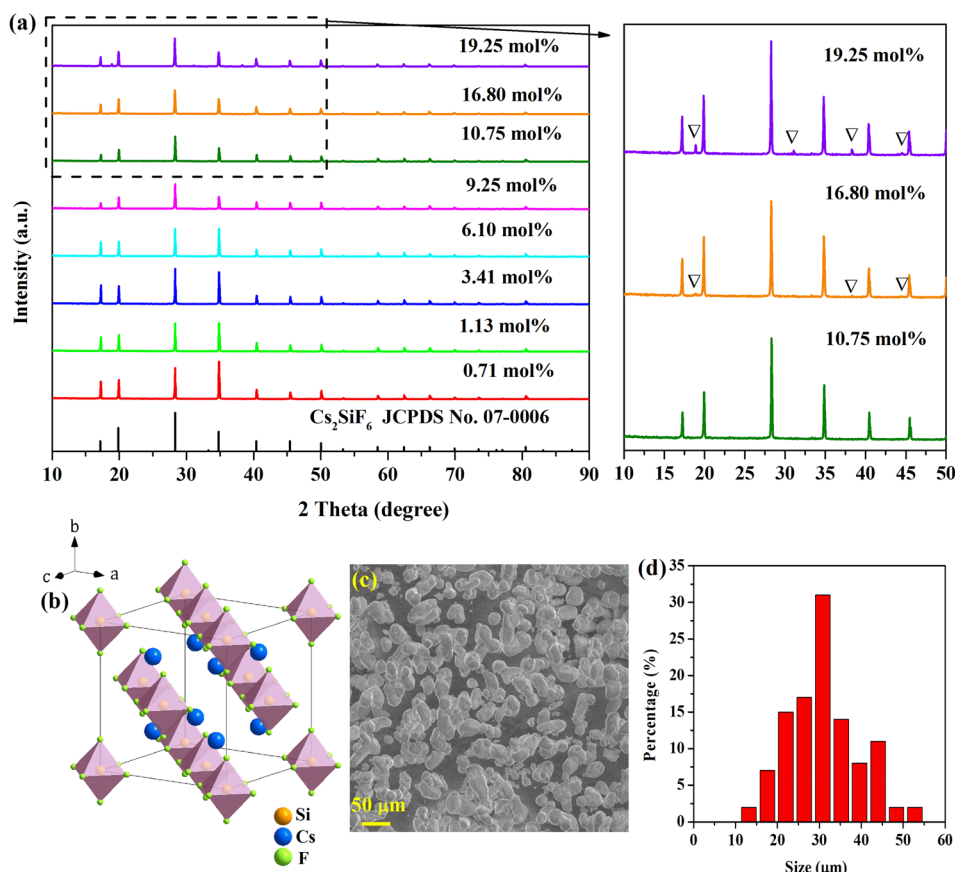


Figure 1. (a) XRD patterns of various Mn^{4+} concentration doped $\text{Cs}_2\text{SiF}_6:\text{Mn}^{4+}$ samples. (b) Crystal structure of Cs_2SiF_6 . (c) SEM and (d) particle size distribution of $\text{Cs}_2\text{SiF}_6:\text{Mn}^{4+}$. The standard card (Cs_2SiF_6) JCPDS No. 07-0006 is included for comparison.

value, but the Mn^{4+} ion doped system usually shows a lower optimal content (<8 mol %), and further increasing the concentration would inevitably result in concentration quenching.³⁵

Here, we report the first realization of an ultrahigh EQE of 71% in Mn^{4+} -doped fluoride phosphor upon 460 nm excitation. For this purpose, we use $\text{Cs}_2\text{SiF}_6:\text{Mn}^{4+}$ with a relatively high doping concentration. Despite that the Jahn–Teller effect of Mn^{4+} ions, electron-vibration effects, and intensities of vibronic transitions in $\text{Cs}_2\text{SiF}_6:\text{Mn}^{4+}$ have been extensively investigated, little attention has been focused on its quantum efficiency (QE) and performances in W-LEDs.^{36–39} It is observed that the optimal concentration of Mn^{4+} in Cs_2SiF_6 is as high as 10.75 mol %. The effects of dopant concentration and temperature on photoluminescence, decay behavior, QE, and AE have been investigated in detail. A mechanistic view is obtained from a combination of static and dynamic spectroscopy and density functional theory (DFT) calculations. By employing the efficient $\text{Cs}_2\text{SiF}_6:\text{Mn}^{4+}$ as red phosphor, we realized a high-performance high-power warm W-LED (power rating of 10 W) with low CCT (3205 K), high CRI ($R_a = 85$; $R_9 = 78$), and luminous efficacy of 111 lm/W under related 300 mA drive current, which presents a substantial advance toward its commercial application.

RESULTS AND DISCUSSION

Figure 1a shows the XRD patterns of different Mn^{4+} concentrations doped $\text{Cs}_2\text{SiF}_6:\text{Mn}^{4+}$ phosphor samples. As the doping concentration of Mn^{4+} is not higher than 10.75 mol

%, all diffraction peaks of the samples match well with the standard card JCPDS No.07-0006, indicating pure phase objective samples of $\text{Cs}_2\text{SiF}_6:\text{Mn}^{4+}$ have been obtained. No impurity or extra peaks were detected in the sample. Together with intense red emission from $\text{Cs}_2\text{SiF}_6:\text{Mn}^{4+}$ (see Figure S1), it can be concluded that different concentrations of Mn^{4+} ions have been incorporated into fluoride Cs_2SiF_6 , while, as the Mn^{4+} concentration was increased to 16.8 mol % or above, some impurity peaks would appear in the samples. Thus, the maximum effective doping concentration of Mn^{4+} ions in Cs_2SiF_6 is 10.75 mol % in our design. Figure 1b shows that Cs_2SiF_6 belongs to a cubic structure with the $Fm\bar{3}m$ space group (225), and the lattice constant is $a = 8.919$ Å. In this structure, there exists only one type of octahedral Si^{4+} ions. Due to the similar valence states and ionic radii between Si^{4+} ($r = 0.40$ Å) and Mn^{4+} ($r = 0.53$ Å), the Mn^{4+} ions would substitute the Si^{4+} ions in $\text{Cs}_2\text{SiF}_6:\text{Mn}^{4+}$.⁴⁰ The typical SEM image in Figure 1c shows that $\text{Cs}_2\text{SiF}_6:\text{Mn}^{4+}$ is composed of some irregular particles with a size of 10–50 μm , and the average size is about ~ 31 μm (see Figure 1d).

Figure 2a shows the room-temperature emission and excitation spectra of $\text{Cs}_2\text{SiF}_6:\text{Mn}^{4+}$. It is observed that the emission spectrum upon 357 or 462 nm excitation consists of six typical sharp emission peaks centered at 600, 610, 614, 632, 636, and 648 nm, originating from the transitions of anti-Stokes $v_3(t_{1u})$, $v_4(t_{1u})$, and $v_6(t_{2u})$ and Stokes $v_6(t_{2u})$, $v_4(t_{1u})$, and $v_3(t_{1u})$ vibronic modes, respectively.⁴¹ The slight red-shift for the emission (Figure 2b) and excitation (Figure S2) peaks as compared to that of $\text{K}_2\text{SiF}_6:\text{Mn}^{4+}$ or $\text{Rb}_2\text{SiF}_6:\text{Mn}^{4+}$ is ascribed to the weaker crystal field strength for Mn^{4+} ions in

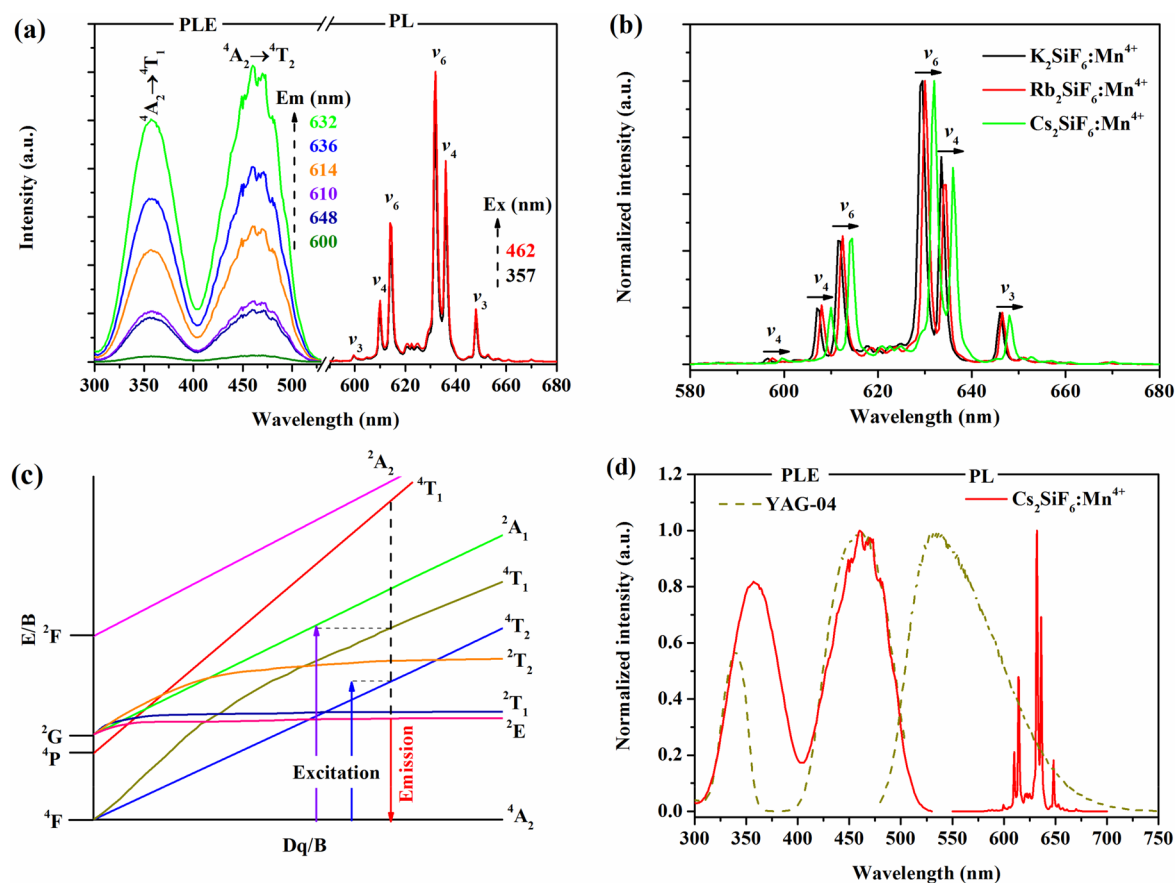


Figure 2. (a) Excitation and emission spectra of $\text{Cs}_2\text{SiF}_6:\text{Mn}^{4+}$, (b) normalized emission spectra of $\text{X}_2\text{SiF}_6:\text{Mn}^{4+}$ ($\text{X} = \text{K}, \text{Rb}, \text{and Cs}$), (c) Tanabe–Sugano energy diagram for $\text{Mn}^{4+}(3d^3)$ in an octahedral crystal field, and (d) normalized emission and excitation spectra of $\text{Cs}_2\text{SiF}_6:\text{Mn}^{4+}$ and YAG-04.

$\text{Cs}_2\text{SiF}_6:\text{Mn}^{4+}$ (Figure 2c).²⁰ Monitoring at these different emission peaks, quite similar excitation spectra are obtained and all of them are composed of two broadband excitation peaks located at ~ 357 and 462 nm, which can be attributed to the spin-allowed $^4\text{A}_2 \rightarrow ^4\text{T}_1$ and $^4\text{A}_2 \rightarrow ^4\text{T}_2$ transitions of Mn^{4+} , respectively. The analogous excitation profiles also suggest that all emission peaks come from a single emission center, which is consistent with the analysis of Mn^{4+} substitution above. Figure 2d shows the normalized emission and excitation spectra of YAG-04 and $\text{Cs}_2\text{SiF}_6:\text{Mn}^{4+}$. As shown, very small overlap between the excitation of $\text{Cs}_2\text{SiF}_6:\text{Mn}^{4+}$ and emission of YAG-04 can be observed, suggesting that the reabsorption problem between the two phosphors would not occur. In addition, the predominant blue excitation bands of $\text{Cs}_2\text{SiF}_6:\text{Mn}^{4+}$ and YAG-04 are almost fully overlapped. These facts strongly confirm that $\text{Cs}_2\text{SiF}_6:\text{Mn}^{4+}$ may act as a red light component for improving the performance of blue InGaN chip excited W-LEDs.

For optimizing the luminescent properties, doped red phosphors $\text{Cs}_2\text{SiF}_6:\text{Mn}^{4+}$ with different Mn^{4+} concentrations have been synthesized (Table 1), and the corresponding emission spectra are given in Figure 3a. It can be observed that all emission spectra consist of several sharp emission peaks located between 550 and 700 nm, corresponding to the $^2\text{E}_g \rightarrow ^4\text{A}_2$ transitions of Mn^{4+} . With the increased Mn^{4+} concentration, the band shape and peak positions of these emission peaks exhibit no changes (see Figure 3b), whereas the emission intensity varied greatly. The detail concentration-dependent

Table 1. AAS Results of Mn^{4+} Ion Doped Cs_2SiF_6 Phosphors Prepared with Different Mole Ratios of K_2MnF_6 to SiO_2 ^a

sample	mole ratio of K_2MnF_6 to SiO_2	Mn^{4+} concentration (mol %)
S1	1:100	0.71
S2	2:100	1.13
S3	5:100	3.41
S4	10:100	6.10
S5	15:100	9.25
S6	20:100	10.75
S7	30:100	16.80
S8	40:100	19.25

^aThe mole ratio of CsF to SiO_2 is fixed at 5:1.

emission intensity is provided in Figure 3d. Apparently, the emission intensity of the sample is increased first with increasing Mn^{4+} concentration and reached its maximum value as the Mn^{4+} concentration rose to ~ 10.75 mol %, and very intense absorption can be found in this phosphor composition, as shown in Figure S3. When the concentration of Mn^{4+} is further increased, the emission intensity of the sample gradually dropped due to the concentration quenching effect and the effects of extra purity phases. Thus, the optimal doping concentration in this system is ~ 10.75 mol %. This value is much higher than that of $\text{K}_2\text{TiF}_6:\text{Mn}^{4+}$ (5.5 mol %),² $\text{Cs}_2\text{GeF}_6:\text{Mn}^{4+}$ (8.78 mol %),³⁵ $\text{K}_3\text{AlF}_6:\text{Mn}^{4+}$ (3.51 mol %),³¹ etc. Figure 3c shows the concentration-dependent luminescence decay curves of Mn^{4+} (monitored at ~ 632 nm) in $\text{Cs}_2\text{SiF}_6:\text{Mn}^{4+}$ upon 460 nm excitation. It can be seen that all

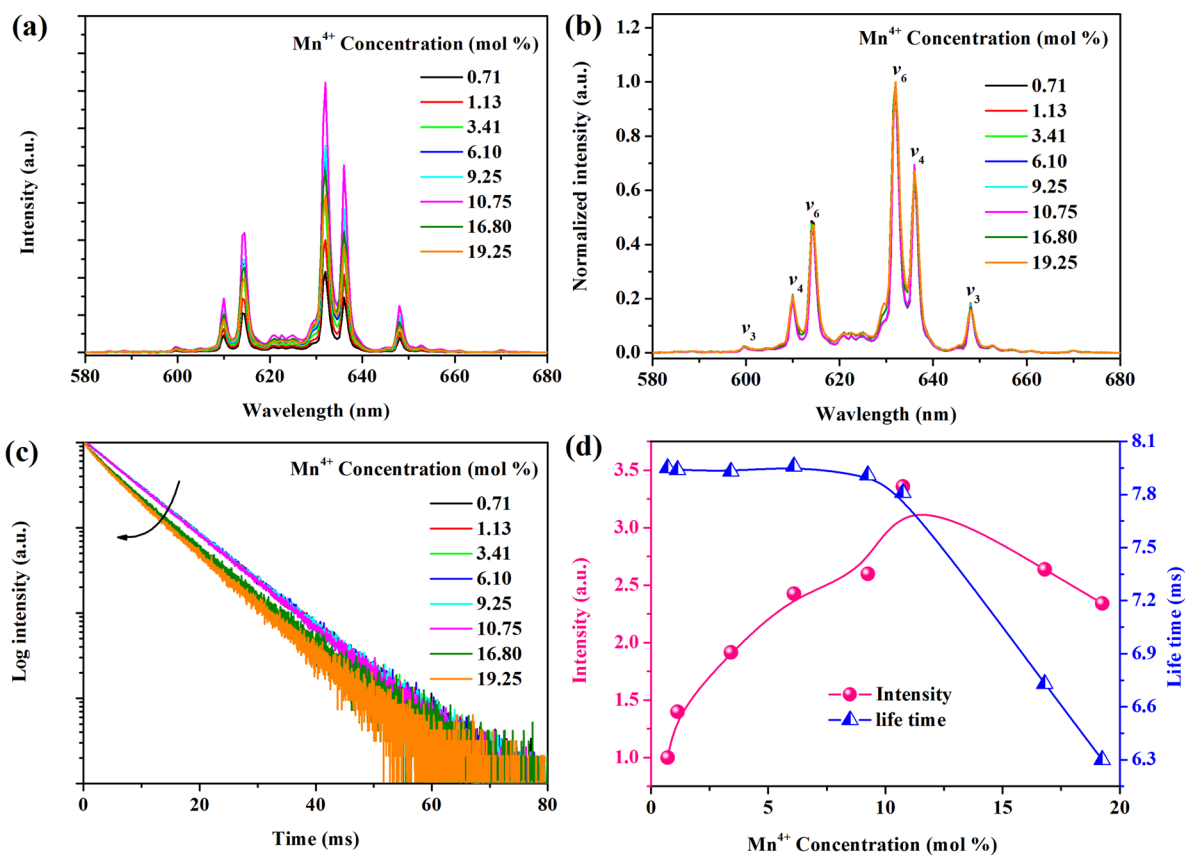


Figure 3. Room-temperature (a) emission and (b) normalized emission spectra, (c) luminescence decay curves (monitored at 632 nm), and (d) integrated intensity and lifetimes of Mn⁴⁺ in Cs₂SiF₆:Mn⁴⁺ with various Mn⁴⁺ concentrations.

luminescence decay curves fit well with a single-exponential equation, which indicates that Mn⁴⁺ ions may tend to distribute homogeneously in host lattice Cs₂SiF₆. As the Mn⁴⁺ concentration increases, the luminescence lifetime exhibited a monotonically decreasing trend. As the Mn⁴⁺ concentration was increased from 0.71 to 10.75 mol %, the lifetime was only reduced by ~0.14 ms and a long lifetime of ~7.81 ms was obtained in Cs₂SiF₆:10.75 mol %Mn⁴⁺. When the concentration of Mn⁴⁺ was further increased to 19.25 mol %, the lifetime of Mn⁴⁺ was decreased to ~6.3 ms. The faster falling rate of lifetime after 10.75 mol % is due to the enhanced nonradiative transition processes among Mn⁴⁺ ions, which is in accord with the concentration quenching behavior. The single-exponential decay behavior and long decay lifetimes for Mn⁴⁺ ions in Cs₂SiF₆:Mn⁴⁺ obviously show that weak Mn⁴⁺–Mn⁴⁺ interactions among Mn⁴⁺ ions in this system and the Mn⁴⁺ ions tend to evenly distribute in the host lattice Cs₂SiF₆. Because of these, a very high optimal concentration for Mn⁴⁺ has been achieved in Cs₂SiF₆:Mn⁴⁺.

To further evaluate the dopant distribution and relative structural stability of Mn⁴⁺-doped Cs₂SiF₆, we performed theoretical calculations on the 2 × 2 × 2 supercell of Cs₂SiF₆ with one to four Si⁴⁺ ions replaced by corresponding Mn⁴⁺ ions. To describe it, we have calculated the formation enthalpy $\Delta H(x)$ as^{42,43}

$$\Delta H(x) = E_x - xE_1 - (1 - x)E_0 \quad (1)$$

,where E_x , E_1 , and E_0 are the total energies with a coverage of x , 1, and 0. Herein, x represents the value of the ion number ratio of Mn⁴⁺ to Si⁴⁺. Some optimized lattice constants and total

energies for special coverage values of the models are given in Tables S1–S3. Based on these results and eq 1, the formation enthalpy for Mn⁴⁺-doped Cs₂SiF₆ as a function of coverage is provided in Figure 4a. As shown, when the coverage is lower than 0.10, all formation enthalpy values of the systems are negative, indicating that Mn⁴⁺-doped Cs₂SiF₆ belongs to an exothermic reaction, and all substitution configurations are possible. As coverage was further increased to 0.125, the formation enthalpies are positive, which suggests that the corresponding substitution configurations are unstable. These phenomena are in good agreement with the experimental results shown in Figure 1a. For coverage $x = 0.625$, there are five possible configurations (see Figure S4), and the computational results are listed in Table S2. Since the optimized cell parameters and the crystal structures of all models do not vary significantly between each other, together with the fact that no significant difference in formation enthalpies could be found in the five different models (Figure 4b), it can be concluded that Mn⁴⁺ ions tend to homogeneously distribute in Cs₂SiF₆:Mn⁴⁺. When the coverage is further increased to $x = 0.9375$, there are 14 different models (Figure S5). The optimized cell parameters (Table S3) and the crystal structures of all models (Figure S5) are also very similar; in addition, the differences in formation enthalpies for the 14 models are very small, which can be neglected (Figure 4c). These computational results firmly and clearly demonstrate that Mn⁴⁺ ions tend to homogeneously distribute in Cs₂SiF₆:Mn⁴⁺ when the coverage is even as high as $x = 0.9375$. Hence, a rather high optimal concentration of 10.75 mol % has been obtained in Cs₂SiF₆:Mn⁴⁺.

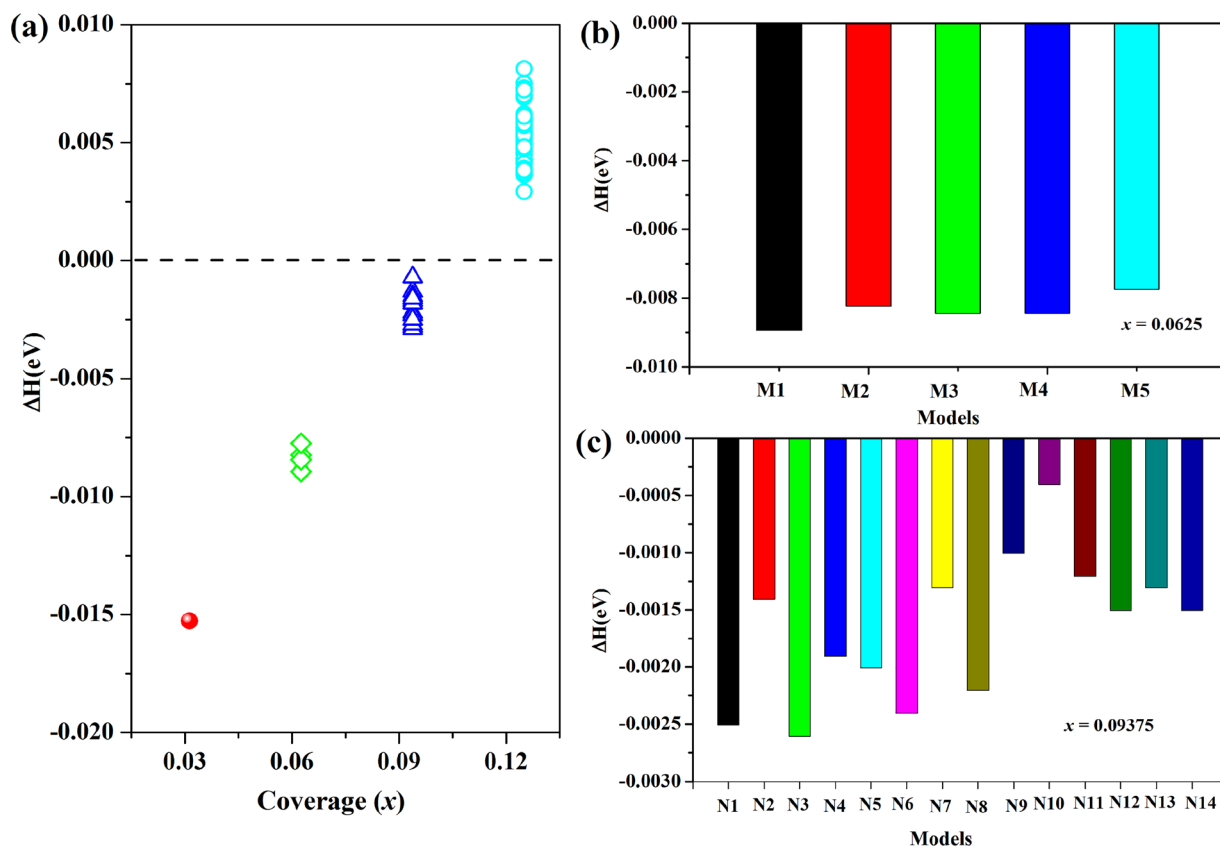


Figure 4. (a) Formation enthalpy for Mn^{4+} substituted for Si^{4+} in a $2 \times 2 \times 2$ Cs_2SiF_6 supercell as a function of coverage (x) and the formation enthalpies for when (b) two ($x = 0.0625$) or (c) three ($x = 0.09375$) Si^{4+} ions are replaced by Mn^{4+} ions in a $2 \times 2 \times 2$ Cs_2SiF_6 supercell under different models.

The quantum efficiency and thermal quenching behavior of the phosphors are both critical factors in evaluating applicability. Hence, we measured the temperature-dependent emission spectra and QE for $\text{Cs}_2\text{SiF}_6:10.75$ mol % Mn^{4+} upon 460 nm excitation. For referencing the QE value, the QE of a commercial high-performance yellow phosphor, YAG:04, was determined with the same experimental setup (upon 460 nm excitation, IQE = 99.73%, EQE = 88.06%; see Figure S6). Figure 5a shows the room-temperature excitation of BaSO_4 and reflectance and emission of $\text{Cs}_2\text{SiF}_6:10.75$ mol %. At room temperature (23 °C), the IQE of $\text{Cs}_2\text{SiF}_6:10.75$ mol % Mn^{4+} could be as high as 89.22% with an AE of 79.96%, resulting in an ultrahigh EQE of 71.34%. The higher AE value is a result of the high Mn^{4+} concentration in this sample. Despite that the IQE value of this phosphor is somewhat lower than that of $\text{K}_2\text{TiF}_6:\text{Mn}^{4+}$ (98%)² and $\text{KNaSiF}_6:\text{Mn}^{4+}$ (90%),²¹ the EQE is much higher than the previously reported Mn^{4+} -doped fluoride red phosphors, such as $\text{K}_2\text{GeF}_6:\text{Mn}^{4+}$ (54%),²² $\text{K}_3\text{AlF}_6:\text{Mn}^{4+}$ (51%),³¹ Rb_2GeF_6 (58%),³⁴ commercial $\text{K}_2\text{SiF}_6:\text{Mn}^{4+}$ (60.6%),³⁴ and $\text{K}_2\text{TiF}_6:\text{Mn}^{4+}$ (56.8%).⁴⁴ Moreover, this value is even larger than that of most nitride phosphors: $(\text{Sr,Ca})_2\text{Si}_3\text{N}_8:\text{Eu}^{2+}$ (60%),⁴⁵ $\text{Sr}_2\text{Si}_3\text{N}_8:\text{Eu}^{2+}$ (64%),⁴⁵ $\text{CaAlSiN}_3:\text{Ce}^{3+}$ (56%),¹⁸ and $(\text{Sr,Ca})\text{AlN}_3:\text{Eu}^{2+}$ (70%).⁴⁶ Such an ultrahigh EQE value is a result of the higher IQE ($\sim 90\%$) and high optimal concentration (10.75 mol %) in $\text{Cs}_2\text{SiF}_6:\text{Mn}^{4+}$. Normally, the higher Mn^{4+} concentration of the phosphor, the higher the AE would be. Herein, the AE is about 80%. In addition, the EQE = IQE \times AE; thus a high EQE value of 71.3% has been obtained in red phosphor $\text{Cs}_2\text{SiF}_6:\text{Mn}^{4+}$ (10.75 mol %) upon 460 nm excitation. In addition, the EQE can be

further improved by optimization of the chemical composition and processing conditions. These facts strongly demonstrate that red phosphor $\text{Cs}_2\text{SiF}_6:\text{Mn}^{4+}$ may have great potential applications in high-power W-LEDs.

Normally, with higher temperature, the QE of the phosphor decreases. For high-power white LED applications, during encapsulation, the processing temperature of the LED chip can reach over ~ 150 °C.⁸ Hence, the temperature-dependent QE of this phosphor has also been investigated, as shown in Table 3 and Figure 5b. When the temperature is gradually increased to 150 °C, the IQE and EQE do not show significant changes, and a high IQE of 85.32% and EQE of 68.58% can be obtained in this phosphor. That is, at 150 °C, the QE of this phosphor has only decreased by less than 5% as compared to that at room temperature (23 °C), exhibiting excellent thermal stability. With further increases in the temperature, both IQE and EQE of this phosphor gradually dropped because of the serious thermal quenching effect. Meanwhile, the AE of the phosphor shows no changes in the whole temperature range (23–300 °C), suggesting that the AE of the phosphor is independent of temperature. As mentioned above, the AE of the phosphor is closely related to the Mn^{4+} concentration. So, it can be deduced that the valence state of Mn^{4+} in $\text{Cs}_2\text{SiF}_6:\text{Mn}^{4+}$ can not be affected by the temperature (23–300 °C). Consequently, when the temperature is gradually cooled to room temperature, the QE could return to its initial value. The temperature-dependent emission spectra and emission intensity are also given in Figure 5c and d, respectively. With increasing temperature, the band shape and peak positions of this phosphor do not vary, whereas the emission intensity changed obviously. In comparison, as the

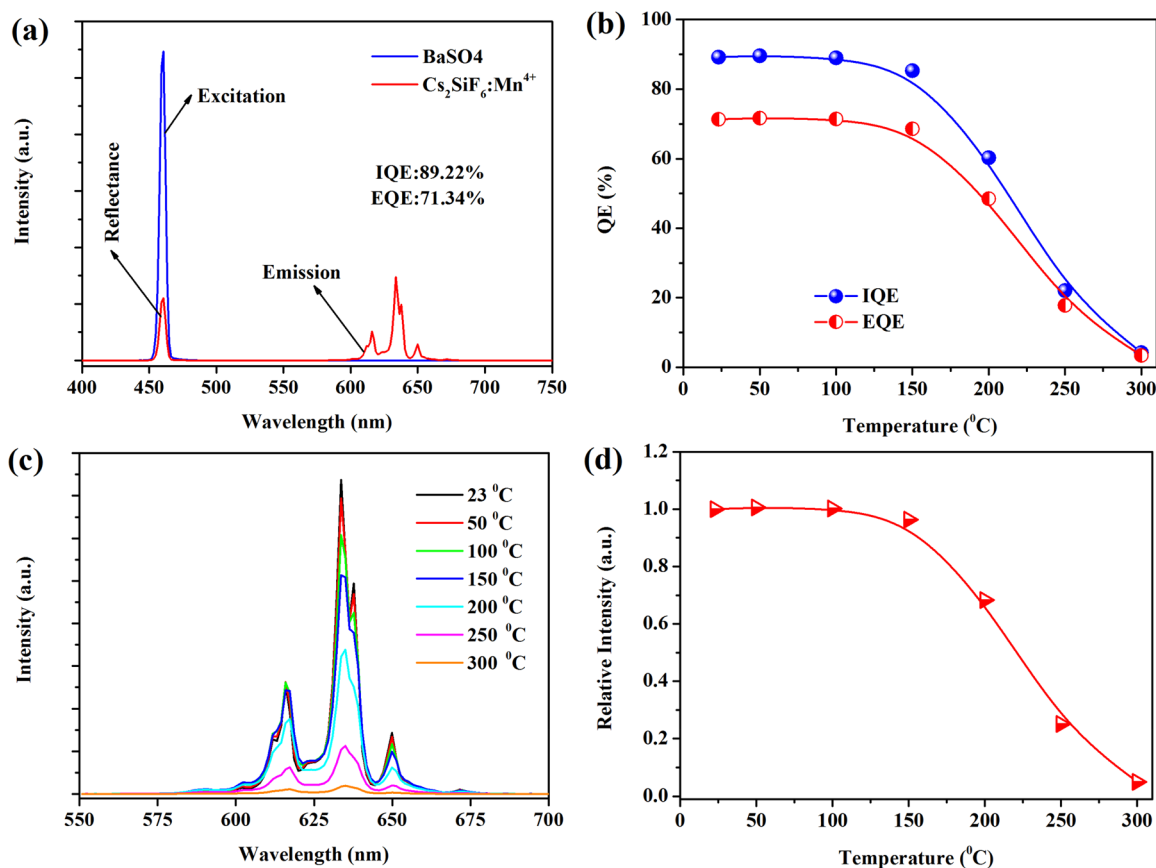


Figure 5. (a) Room-temperature excitation of BaSO₄ and reflection and emission of Cs₂SiF₆:10.75 mol % Mn⁴⁺, (b) temperature-dependent IQE and EQE of Cs₂SiF₆:10.75 mol % Mn⁴⁺ in the range ~23–300 °C, and (c) emission spectra and (d) corresponding integrated emission intensity of Cs₂SiF₆:10.75 mol % Mn⁴⁺ as a function of temperature.

Table 2. Some Photoelectric Parameters of the Fabricated LEDs with a Power Rating of 10 W under a Drive Current of 300 mA

device	Cs ₂ SiF ₆ :Mn ⁴⁺ (wt %)	CCT (K)	Ra	R9	chromaticity coordinate (x, y)	efficacy (lm/W)
LED I	0	6395	72.9	-16.1	(0.3152, 0.3250)	127.72
LED II	20	3762	80.1	44.5	(0.3948, 0.3934)	120.05
LED III	25	3205	85.3	78.1	(0.4248, 0.4029)	111.10
LED IV	30	2748	89.7	98.4	(0.4615, 0.4091)	97.60

^awt/% = mass of Cs₂SiF₆:Mn⁴⁺/mass of epoxy resin × 100%.

Table 3. Temperature-Dependent Absorption Efficiency (AE), Internal Quantum Efficiency (IQE), and External Quantum Efficiency (EQE) of Cs₂SiF₆:10.75 mol % Mn⁴⁺ upon 460 nm Excitation

	temperature (°C)						
	23	50	100	150	200	250	300
AE (%)	79.96	79.99	80.23	80.37	80.52	80.65	80.79
IQE (%)	89.22	89.60	89.00	85.32	60.29	22.08	4.23
EQE (%)	71.34	71.67	71.41	68.58	48.5	17.81	3.42

temperature increases, the emission intensity exhibits a changing trend similar to that of quantum efficiency (Figure 5b). Specifically, at 150 °C, the emission intensity can still remain at ~95% of the initial value at 23 °C. When the temperature further rose to 200 °C, the emission intensity decreased to 68% of the initial value (at ~23 °C). These facts strongly indicate that red phosphor Cs₂SiF₆:Mn⁴⁺ has a

superior thermal stability, showing great promise for high-power white LEDs applications.

To further evaluate the commercial application of the synthesized Cs₂SiF₆:Mn⁴⁺ phosphor, the performances of high-power WLEDs with different CCT fabricated with blue InGaN chips, yellow phosphor YAG-04, and red phosphor Cs₂SiF₆:Mn⁴⁺ have been investigated. Figure 6a shows the electroluminescence (EL) spectra of the fabricated W-LEDs (LED I–IV), and Table 2 provides some important photoelectric parameters. Without adding red phosphor, the obtained white LED (LED I) shows a higher CCT (6359 K) and lower color rendering index (Ra = 72.9; R9 = -16.1) due to the deficient red emission component from yellow phosphor YAG-04. However, as the red phosphor Cs₂SiF₆:Mn⁴⁺ was added into the devices, the EL of the fabricated LEDs (LED II–IV) consisted of three typical emission parts: blue emission from the InGaN chip, yellow emission from YAG-04, and sharp red emission from Cs₂SiF₆:Mn⁴⁺. Due to the different emission intensity ratio of the three parts in the devices, white LEDs (LED II–IV) with different CCT and color rendering index can

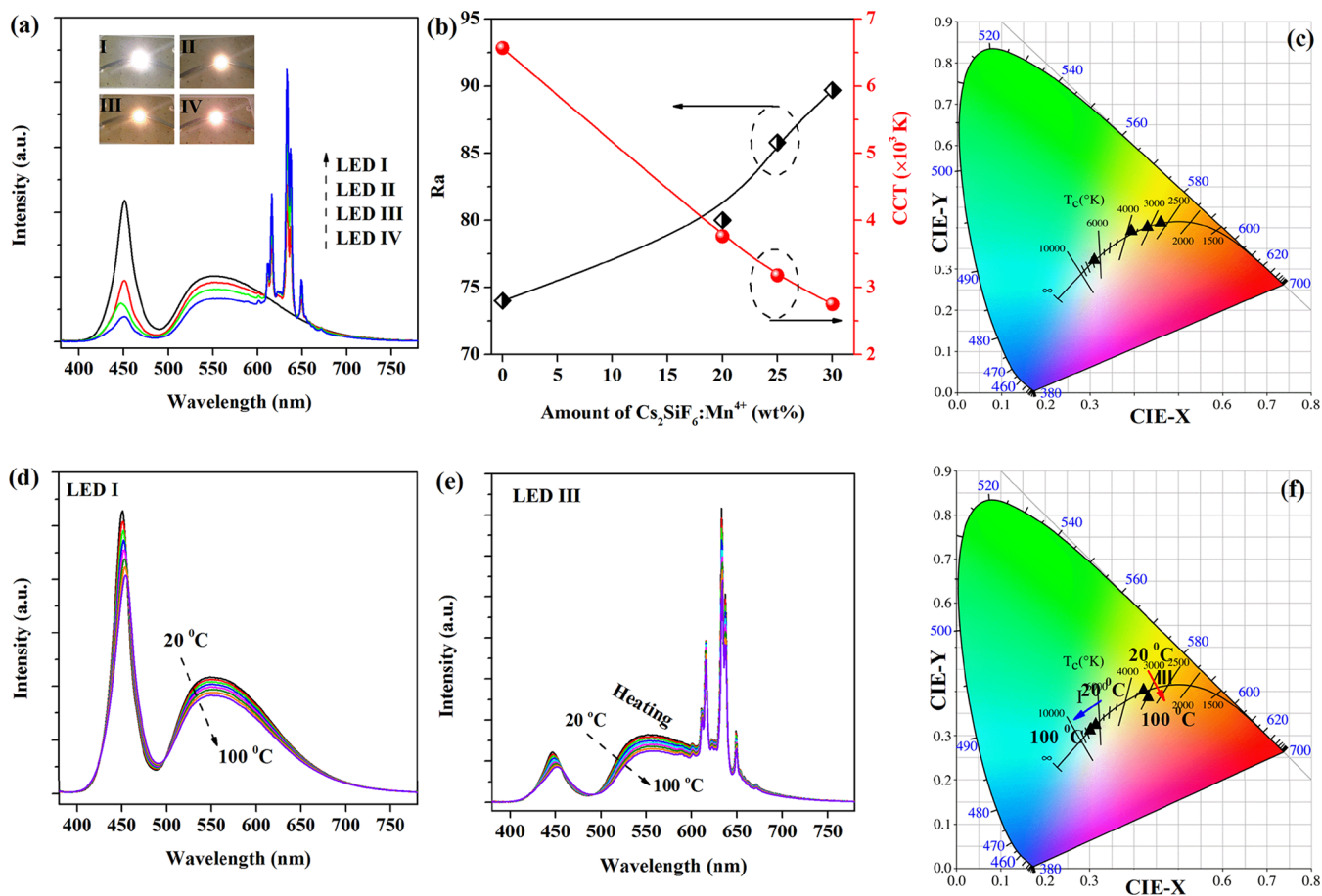


Figure 6. (a) Electroluminescence spectra and (b) CCT and Ra of the fabricated high-power white LEDs with different mass ratios of YAG04 to red phosphor $\text{Cs}_2\text{SiF}_6:\text{Mn}^{4+}$, (c) corresponding CIE chromaticities in the 1931 CIE diagram, temperature-dependent electroluminescence spectra (d, e), and (f) corresponding CIE chromaticities in the 1931 CIE diagram for LED I and LED III.

be obtained, and all of them are located in the warm white light region (see Figure 6c). As shown in Figure 6b, with an increase in red phosphor $\text{Cs}_2\text{SiF}_6:\text{Mn}^{4+}$ from 0 to 30 wt %, the CCT sharply decreased from 6359 K to 2748 K, while the Ra improved from 73 to 90 due to the gradually increasing red light component from $\text{Cs}_2\text{SiF}_6:\text{Mn}^{4+}$. In addition, the R9 value has also been significantly improved from ~ -16 to 99. Despite that the luminous efficacy of warm white LEDs shows some decrease as compared to cool white LED I, high-power warm white LEDs with a luminous efficacy of ~ 98 – 120 lm/W could be easily realized, exhibiting great promise for practical applications.

In addition, the effects of high temperature on the performances of the white LEDs have also been investigated. Figure 6d and e show the temperature-dependent EL spectra of LED I and III, respectively. For LED I, all emission spectra contain blue and yellow emission bands, corresponding to the InGaN chip and yellow phosphor YAG-04, respectively. With an increase in temperature, both blue and yellow emissions monotonically declined because of the thermal quenching effect. As the blue InGaN chip and yellow phosphor has different descent speeds, the white light point would blue-shift slightly with increasing temperature (see Figure 6f). Accordingly, the CCT could be increased from 6395 K (20 °C) to 7095 K (100 °C) (see Table 4). Meanwhile, when the temperature was increased to 100 °C, the luminous efficacy of LED I was reduced to $\sim 75\%$ of its initial value (20 °C). Furthermore, as

Table 4. Temperature-Dependent Parameters of LED I under a Drive Current of 300 mA

temperature (°C)	CCT (K)	Ra	R9	chromaticity coordinate (x, y)	efficiency (lm/W)
20	6395	72.9	-16.1	(0.3152, 0.3250)	127.72
30	6446	73.4	-14.6	(0.3144, 0.3240)	122.88
40	6500	73.9	-13.2	(0.3136, 0.3231)	117.86
50	6563	74.4	-11.9	(0.3126, 0.3222)	116.91
60	6627	74.9	-10.6	(0.3117, 0.3213)	114.43
70	6699	75.4	-9.2	(0.3106, 0.3202)	112.02
80	6782	75.9	-7.9	(0.3094, 0.3191)	109.27
90	6880	76.4	-6.4	(0.3081, 0.3178)	106.60
100	7035	77.1	-4.5	(0.3060, 0.3156)	95.61

the InGaN chip and YAG-04 exhibit different change trends with increasing temperature, both Ra and R9 would also be slightly increased, and the details are shown in Table 4. In comparing with LED I, warm white LED III exhibited a different changing trend with rising temperature. As shown in Figure 6e, with an increase in temperature, all emissions of LED III would gradually decrease because of the thermal quenching effect. Since the three typical emission parts have different thermal quenching behaviors, the white color point of LED III was also shifted, but giving a different shift direction, as shown in Figure 6f. Consequently, when the temperature was increased from 20 °C to 100 °C, the CCT was decreased from 3205 K to 2931 K, which is obviously different from LED

I. Meanwhile, the luminous efficacy of LED III was decreased by ~21%, which clearly indicates that the thermal quenching behavior of LED I is more serious than that of LED III. In addition, both Ra and R9 have been obviously improved (see Table 5). The enhanced high-temperature performance of the

Table 5. Temperature-Dependent Parameters of the LED III under a Drive Current of 300 mA

temperature (°C)	CCT (K)	Ra	R9	chromaticity coordinate (x, y)	efficacy (lm/W)
20	3205	85.3	78.1	(0.4248, 0.4029)	111.10
30	3172	85.8	79.4	(0.4259, 0.4013)	109.08
40	3134	86.5	80.7	(0.4271, 0.3993)	106.52
50	3093	87.2	82.3	(0.4284, 0.3973)	103.62
60	3055	87.8	83.5	(0.296, 0.3953)	100.79
70	3020	88.4	84.5	(0.4307, 0.3934)	97.83
80	2986	89.0	85.5	0.4316, 0.3913)	94.79
90	2955	89.6	86.2	(0.4324, 0.3893)	91.53
100	2931	90.2	86.7	(0.4327, 0.3872)	87.97

LED is due to the high EQE (~71%) and excellent thermal stability of red phosphor Cs₂SiF₆:Mn⁴⁺. Based on these, it can be concluded that Cs₂SiF₆:Mn⁴⁺ may be used as an efficient red component in high-power warm W-LEDs.

CONCLUSIONS

In summary, a series of Mn⁴⁺ ion doped narrow-band emitting fluoride red phosphors Cs₂SiF₆:Mn⁴⁺ have been synthesized via a facile co-precipitation method at room temperature. The phosphor shows strong broadband absorption at ~460 nm and high-purity sharp red emission around ~630 nm, which matches well with the emission light of InGaN blue chip. By optimizing the doping concentration, phosphor composition Cs₂SiF₆:Mn⁴⁺ (10.75 mol %) provides a high IQE of 89% and ultrahigh EQE of 71% upon 460 nm excitation. In addition, at 150 °C, both IQE and EQE could remain at nearly ~95% of their initial room-temperature values, showing superior thermal stability. The luminescent measurements and DFT calculations show that the performance of Cs₂SiF₆:Mn⁴⁺ is attributed to Mn⁴⁺ ions tending to homogeneously distribute into the host lattice Cs₂SiF₆. By using the highly efficient and thermally stable phosphor Cs₂SiF₆:Mn⁴⁺ (10.75 mol %) as a red light component, a high-power warm white LED with high CRI (Ra = 85, R9 = 78), low CCT (3205 K), and a high luminous efficacy of 110 lm/W under rated 300 mA drive current could be obtained. These findings show the great promise of Cs₂SiF₆:Mn⁴⁺ as a commercial red phosphor in high-power warm white LEDs.

EXPERIMENTAL SECTION

Materials Synthesis. Red phosphor Cs₂SiF₆:Mn⁴⁺ was synthesized via a co-precipitation method as described elsewhere.³² The raw materials are SiO₂ (99.8%), CsF (99.9%), HF (49 wt %), KMnO₄ (99.3%), acetone (AR), and H₂O₂ (30 wt %); all of them were used as obtained without further purification. The key precursor K₂MnF₆ was synthesized using the Bode's method.⁴⁷ For safety consideration, necessary safeguard procedures (glove, patch, draft cupboard, etc.) are required in the synthesis processes. The synthesis diagram for Cs₂SiF₆:Mn⁴⁺ is given in Figure S1. In a typical procedure, 0.3 g of SiO₂ was dissolved in 10 mL of HF (49 wt %) in a 50 mL plastic beaker to form a colorless and transparent solution; then

0.0247 g of K₂MnF₆ was added into the above solution under stirring. After the precursor K₂MnF₆ was fully dissolved, 3.79 g of CsF was added into the solution, which was further stirred for 30 min. The red phosphor Cs₂SiF₆:Mn⁴⁺ was gradually generated. Then, the solution was aged 2 h in an ice bath. Herein, the ice bath is used to reduce the volatilization of toxic HF and simultaneously prevent the valence state change of Mn⁴⁺ in the synthesis processes. The collected products were washed three times with acetone and finally dried at 80 °C for 2 h under a vacuum environment for further characterization. For optimizing the luminescence properties, different Mn⁴⁺ concentration doped Cs₂SiF₆:Mn⁴⁺ samples were further synthesized by controlling the mole ratios of SiO₂ to K₂MnF₆, as shown in Table 1. Other pure phase phosphors, Rb₂SiF₆:Mn⁴⁺ and K₂SiF₆:Mn⁴⁺, could be obtained by the same synthesis procedures (Figure S7).

Materials Characterization. The crystal structures of the synthesized samples were characterized by using a Philips model PW1830 X-ray powder diffractometer with Cu K α radiation ($\lambda = 1.5406 \text{ \AA}$), and the tube voltage and current are 40 kV and 40 mA, respectively. The morphology and size of the samples were determined by a scanning electron microscope (SEM, NOANOSEM 430). The room- or high-temperature photoluminescence (PL) and photoluminescence excitation (PLE) spectra, as well as fluorescence decay curves, were detected by an FL920 fluorescence spectrophotometer (Edinburgh Instruments LTD) using a 450 W xenon lamp or a 150 W μ s flash lamp as the excitation source. The diffuse reflection spectra of the samples were collected by a UV2600 spectrophotometer (Shimadzu). The compositional analysis was performed on a Shimadzu AA-6300 absorption spectrophotometer (AAS). The temperature-dependent absorption efficiency and internal and external quantum efficiencies of the sample were measured by a QE-2100 spectrophotometer (Otsuka Electronics, Japan). The AE, IQE, and EQE were calculated by using the following equations:⁴⁸

$$AE = \frac{\int \lambda \{E(\lambda) - R(\lambda)\} d\lambda}{\int \lambda \cdot E(\lambda) d\lambda} \quad (2)$$

$$IQE = \frac{\int \lambda \cdot P(\lambda) d\lambda}{\int \lambda \{E(\lambda) - R(\lambda)\} d\lambda} \quad (3)$$

$$EQE = IQE \times AE = \frac{\int \lambda \cdot P(\lambda) d\lambda}{\int \lambda \cdot E(\lambda) d\lambda} \quad (4)$$

where $E(\lambda)/h\nu$, $R(\lambda)/h\nu$, and $P(\lambda)/h\nu$ are the number of photons in the spectrum of excitation, reflectance, and emission of the phosphor, respectively.

Theoretical Calculations. Theoretical calculations were performed through DFT implemented in the Vienna *ab initio* simulation package (vasp).^{49–51} The exchange correlation potential was approximated by the generalized gradient approximation (GGA) with the PBE functional.⁵² To evaluate the Mn⁴⁺ distribution in Cs₂SiF₆:Mn⁴⁺, a 2 × 2 × 2 Cs₂SiF₆ supercell and a 2 × 2 × 2 Cs₂MnF₆ were adopted according to the ICSD cards No. 94089 or 47201, and the optimized parameters are shown in Table S1. When two Si⁴⁺ ions were replaced by two Mn⁴⁺ ions in the optimized 2 × 2 × 2 Cs₂SiF₆ supercell, there were five different configurations (Figure S4), while when three and four Si⁴⁺ ions are substituted by Mn⁴⁺

ions in this supercell, there are 14 (Figure S5) and 71 different configurations, respectively.^{53,54} The cutoff energy E_{cut} and K-point mesh were set as 520 eV with a $2 \times 2 \times 2$ Monkhorst–Pack grid, which are enough for energy convergence. The convergence criterion for the electronic energy was 10^{-4} eV, and the structures were relaxed until the Hellmann–Feynman forces were less than 0.02 eV \AA^{-1} .

LED Fabrication and Performance Measurement.

High-power W-LEDs were fabricated with a commercial yellow phosphor YAG:Ce³⁺ (YAG04, intermax), the present red phosphor Cs₂SiF₆:Mn⁴⁺, and blue InGaN chips (450–460 nm, 200 mW, Tsinghua Tongfang). The blue chips were fixed on a substrate with a diameter of 11.2 cm using the chip-on-board technology.³¹ The phosphors were thoroughly mixed with epoxy resin, and the obtained phosphor–epoxy resin mixture was coated on the LED chips. Four white LEDs (LED I–IV) with different CCTs were fabricated with different mass ratios of the epoxy resin (A, B) to the phosphors (YAG04, Cs₂SiF₆:Mn⁴⁺); details are given in Table 2. The photoelectric properties of the LEDs at various temperatures were measured by using an integrating sphere spectroradiometer system (ATA100, Everfine).

■ ASSOCIATED CONTENT

Supporting Information

The Supporting Information is available free of charge on the ACS Publications website at DOI: 10.1021/acsphtonic.7b00852.

Tables S1–S3 and Figures S1–S7; additional DFT calculation results; synthesis diagram; excitation spectra; diffuse reflection spectrum; DFT calculation models; quantum efficiency; XRD patterns (PDF)

■ AUTHOR INFORMATION

Corresponding Authors

*E-mail: scxbyang@scut.edu.cn.

*E-mail: qyzhang@scut.edu.cn.

ORCID

Shi Ye: 0000-0001-9625-8222

Qinyuan Zhang: 0000-0001-6544-4735

Notes

The authors declare no competing financial interest.

■ ACKNOWLEDGMENTS

This research was financially supported by the National Science Foundation of China (Grant Nos. 51472088, 51602104, and U1601205), Fundamental Research Funds for the Central Universities (No. D2174710), and the Natural Science Foundation of Guangdong Province (No. 2015A030310526).

■ REFERENCES

- (1) Ye, S.; Xiao, F.; Pan, Y. X.; Ma, Y. Y.; Zhang, Q. Y. Phosphors in Phosphor-Converted White Light-Emitting Diodes: Recent Advances in Materials, Techniques and Properties. *Mater. Sci. Eng., R* **2010**, *71*, 1–34.
- (2) Zhu, H. M.; Lin, C. C.; Luo, W. Q.; Shu, S. T.; Liu, Z. G.; Liu, Y.; Kong, J. T.; Ma, E.; Cao, Y. G.; Liu, R. S.; Chen, X. Y. Highly Efficient Non-Rare-Earth Red Emitting Phosphor for Warm White Light-Emitting Diodes. *Nat. Commun.* **2014**, *5*, 4312–4321.
- (3) Daicho, H.; Iwasaki, T.; Enomoto, K.; Sasaki, Y.; Maeno, Y.; Shinomiya, Y.; Aoyagi, S.; Nishibori, E.; Sakata, M.; Sawa, H. A Novel

Phosphor for Glareless White Light-Emitting Diodes. *Nat. Commun.* **2012**, *3*, 1132–1139.

- (4) Pust, P.; Weiler, V.; Hecht, C.; Tücks, A.; Wochnik, A. S.; Henß, A.; Wiechert, D.; Scheu, C.; Schmidt, P. J.; Schnick, W. Narrow-Band Red-Emitting Sr[LiAl₃N₄]:Eu²⁺ as a Next-generation LED-Phosphor Material. *Nat. Mater.* **2014**, *13*, 891–896.

- (5) Schubert, E. F.; Kim, J. K. Solid-State Light Sources Getting Smart. *Science* **2005**, *308*, 1274–1278.

- (6) Zhang, X. J.; Yu, J. B.; Wang, J.; Lei, B. F.; Liu, Y. L.; Cho, Y. J.; Xie, R. J.; Zhang, H. W.; Li, Y. R.; Tian, Z. F.; Li, Y.; Su, Q. All-Inorganic Light Converter Based on Phosphor-in-Glass Engineering for Next-Generation Modular High-Brightness White LEDs/LDs. *ACS Photonics* **2017**, *4*, 986–995.

- (7) Zeuner, M.; Schmidt, P. J.; Schnick, W. One-Pot Synthesis of Single-Source Precursors for Nanocrystalline LED Phosphors M₂Si₂N₈:Eu²⁺ (M = Sr, Ba). *Chem. Mater.* **2009**, *21*, 2467–2473.

- (8) Huang, L.; Zhu, Y. W.; Zhang, X. J.; Zou, R.; Pan, F. J.; Wang, J.; Wu, M. M. HF-Free Hydrothermal Route for Synthesis of Highly Efficient Narrow-Band Red Emitting Phosphor K₂Si_{1-x}F_{6-x}Mn⁴⁺ for Warm White Light-Emitting diodes. *Chem. Mater.* **2016**, *28*, 1495–1502.

- (9) Wang, Z. B.; Chu, I. H.; Zhou, F.; Ong, S. P. Electronic Structure Descriptor for Discovery of Narrow-Band Red-Emitting Phosphors. *Chem. Mater.* **2016**, *28*, 4024–4031.

- (10) Wang, B.; Lin, H.; Huang, F.; Xu, J.; Chen, H.; Lin, Z. B.; Wang, Y. S. Non-Rare-Earth BaMgAl_{10-2x}O₁₇:xMn⁴⁺,xMg²⁺: a Narrow-band Red Phosphor for High-Power Warm W-LED. *Chem. Mater.* **2016**, *28*, 3515–3524.

- (11) Jin, Y. H.; Hu, Y. H.; Wu, H. Y.; Duan, H.; Chen, L.; Fu, Y. R.; Ju, G. F.; Mu, Z. F.; He, M. A Deep Red Phosphor Li₂MgTiO₄:Mn⁴⁺ Exhibiting Abnormal Emission: Potential Application As Color Converter for Warm W-LEDs. *Chem. Eng. J.* **2016**, *288*, 596–607.

- (12) Lin, C. C.; Meijerink, A.; Liu, R. S. Critical Red Components for Next-Generation White LEDs. *J. Phys. Chem. Lett.* **2016**, *7* (3), 495–503.

- (13) Wang, B.; Lin, H.; Xu, J.; Chen, H.; Wang, Y. S. CaMg₂Al₁₆O₂₇:Mn⁴⁺-based Red Phosphor: A potential Color Converter for High-Powered Warm W-LED. *ACS Appl. Mater. Interfaces* **2014**, *6*, 22905–22913.

- (14) Xia, Z. G.; Xu, Z. H.; Chen, M. Y.; Liu, Q. L. Recent Developments in the New Inorganic Solid-State LED Phosphors. *Dalton Trans.* **2016**, *45*, 11214–11232.

- (15) Xia, Z. G.; Liu, Q. L. Progress in Discovery and Structural Design of Color Conversion Phosphors for LEDs. *Prog. Mater. Sci.* **2016**, *84*, 59–117.

- (16) Li, H. L.; Xie, R. J.; Hirosaki, N.; Takeda, T.; Zhou, G. H. Synthesis and luminescence properties of orange–red-emitting M₂Si₂N₈:Eu²⁺ (M = Ca, Sr, Ba) Light-Emitting Diode Conversion Phosphors by a Simple Nitridation of MSi₂. *Int. J. Appl. Ceram. Technol.* **2009**, *6*, 459–464.

- (17) Peng, M. Y.; Yin, X. W.; Tanner, P. A.; Brik, M. G.; Li, P. F. Site Occupancy Preference, Enhancement Mechanism, and Thermal Resistance of Mn⁴⁺ red Luminescence in Sr₄Al₁₄O₂₅:Mn⁴⁺ for Warm WLEDs. *Chem. Mater.* **2015**, *27*, 2938–2945.

- (18) Li, Y. Q.; Hirosaki, N.; Xie, R. J.; Takeda, T.; Mitomo, M. Yellow-Orange-Emitting CaAlSiN₃:Ce³⁺ Phosphor: Structure, Photoluminescence, and Application in White LEDs. *Chem. Mater.* **2008**, *20*, 6704–6714.

- (19) Piao, X. Q.; Machida, K.; Horikawa, T.; Hanzawa, H.; Shimomura, Y.; Kijima, N. Preparation of CaAlSiN₃:Eu²⁺ Phosphors by the Self-Propagating High-Temperature Synthesis and Their Luminescent Properties. *Chem. Mater.* **2007**, *19*, 4592–4599.

- (20) Paulusz, A. G. Efficient Mn (IV) Emission in Fluorine Coordination. *J. Electrochem. Soc.* **1973**, *120*, 942–947.

- (21) Jin, Y.; Fang, M. H.; Grinberg, M.; Mahlik, S.; Lesniewski, T.; Brik, M. G.; Luo, G. Y.; Lin, J. G.; Liu, R. S. Narrow Red Emission Band Fluoride Phosphor KNaSiF₆:Mn⁴⁺ for Warm White Light-Emitting Diodes. *ACS Appl. Mater. Interfaces* **2016**, *8*, 11194–11203.

- (22) Wei, L. L.; Lin, C. C.; Wang, Y. Y.; Fang, M. H.; Jiao, H.; Liu, R. S. Photoluminescent Evolution Induced by Structural Transformation Through Thermal Treating in the Red Narrow-band Phosphor $K_2GeF_6:Mn^{4+}$. *ACS Appl. Mater. Interfaces* **2015**, *7*, 10656–10659.
- (23) Nguyen, H. D.; Lin, C. C.; Liu, R. S. Waterproof Alkyl Phosphate Coated Fluoride Phosphors for Optoelectronic Materials. *Angew. Chem., Int. Ed.* **2015**, *54*, 10862–10866.
- (24) Nguyen, H.; Lin, C. C.; Fang, M. H.; Liu, R. S. Synthesis of $Na_2SiF_6:Mn^{4+}$ Red Phosphors for White LED Applications by Co-Precipitation. *J. Mater. Chem. C* **2014**, *2*, 10268–10272.
- (25) Fang, M. H.; Nguyen, H.; Lin, C. C.; Liu, R. S. Preparation of a Novel Red $Rb_2SiF_6:Mn^{4+}$ Phosphor with High Thermal Stability Through a Simple One-Step Approach. *J. Mater. Chem. C* **2015**, *3*, 7277–7280.
- (26) Lv, L. F.; Chen, Z.; Liu, G. K.; Huang, S. M.; Pan, Y. X. Optimized Photoluminescence of Red Phosphor $K_2TiF_6:Mn^{4+}$ Synthesized At Room Temperature and Its Formation Mechanism. *J. Mater. Chem. C* **2015**, *3*, 1935–1941.
- (27) Oh, J. H.; Kang, H.; Eo, Y. J.; Park, H. K.; Do, Y. R. Synthesis of Narrow-Band Red-Emitting $K_2SiF_6:Mn^{4+}$ Phosphors for a Deep Red Monochromatic LED and Ultrahigh color Quality Warm-White LEDs. *J. Mater. Chem. C* **2015**, *3*, 607–615.
- (28) Liao, C. X.; Cao, R. P.; Ma, Z. J.; Li, Y.; Dong, G. P.; Sharafudeen, K. N.; Qiu, J. R. Synthesis of $K_2SiF_6:Mn^{4+}$ Phosphor From SiO_2 Powders via Redox Reaction in $HF/KMnO_4$ Solution and Their Application in Warm-white LED. *J. Am. Ceram. Soc.* **2013**, *96*, 3552–3556.
- (29) Wang, Z. L.; Zhou, Y. Y.; Yang, Z. Y.; Liu, Y.; Yang, H.; Tan, H. Y.; Zhang, Q. H.; Zhou, Q. Synthesis of $K_2XF_6:Mn^{4+}$ ($X = Ti, Si$ and Ge) Red Phosphors for White LED Applications with Low-Concentration of HF. *Opt. Mater.* **2015**, *49*, 235–240.
- (30) Wang, Z. L.; Liu, Y.; Zhou, Y. Y.; Zhou, Q.; Tan, H. Y.; Zhang, Q. H.; Peng, J. H. Red-Emitting Phosphors $Na_2XF_6:Mn^{4+}$ ($X = Si, Ge, Ti$) With High Colour-Purity for Warm White-Light-Emitting Diodes. *RSC Adv.* **2015**, *5*, 58136–58140.
- (31) Song, E. H.; Wang, J. Q.; Shi, J. H.; Deng, T. T.; Ye, S.; Peng, M. Y.; Wang, J.; Wondraczek, L.; Zhang, Q. Y. Highly Efficient and Thermally Stable $K_3AlF_6:Mn^{4+}$ as a Red Phosphor for Ultra-High-Performance Warm White Light-Emitting Diodes. *ACS Appl. Mater. Interfaces* **2017**, *9*, 8805–8812.
- (32) Song, E. H.; Wang, J. Q.; Ye, S.; Jiang, X. F.; Peng, M. Y.; Zhang, Q. Y. Room-Temperature Synthesis and Warm-white LEDs Applications of Mn^{4+} Ions Doped Fluoroaluminate Red Phosphor $Na_3AlF_6:Mn^{4+}$. *J. Mater. Chem. C* **2016**, *4*, 2480–2487.
- (33) Deng, T. T.; Song, E. H.; Sun, J.; Wang, L. Y.; Deng, Y.; Ye, S.; Wang, J.; Zhang, Q. Y. The Fesign and Preparation of the Thermally Stable, Mn^{4+} Ion Activated, Narrow band, Red emitting Fluoride $Na_3GaF_6:Mn^{4+}$ for Warm WLED Applications. *J. Mater. Chem. C* **2017**, *5*, 2910–2918.
- (34) Wu, W. L.; Fang, M. H.; Zhou, W. L.; Lesniewski, T.; Mahlik, S.; Grinberg, M.; Brik, M. G.; Sheu, H.; Cheng, B. M.; Wang, J.; Liu, R. S. High Color Rendering Index of $Rb_2GeF_6:Mn^{4+}$ for Light-Emitting Diodes. *Chem. Mater.* **2017**, *29*, 935–939.
- (35) Wang, Z. L.; Zhou, Y. Y.; Liu, Y.; Zhou, Q.; Luo, L. J.; Tan, H. Y.; Zhang, Q. H.; Chen, G.; Peng, J. H. Highly Efficient Red Phosphor $Cs_2GeF_6:Mn^{4+}$ for Warm White light Emitting Diodes. *RSC Adv.* **2015**, *5*, 82409–82414.
- (36) Brik, M. G. Cs_2XF_6 ($X = Si, Ge$) Compounds: Common and Different Features as Uncovered By the First-Principles Calculations. *Solid State Commun.* **2010**, *150*, 1529–1533.
- (37) Manson, N. B.; Hasan, Z.; Flint, C. D. Jahn-Teller Effect in the ${}^4T_{2g}$ State of Mn^{4+} in Cs_2SiF_6 . *J. Phys. C: Solid State Phys.* **1979**, *12*, 5483–5488.
- (38) Campochiaro, C.; McClure, D. S.; Rabinowitz, P.; Dougal, S. Vibronic Coupling in the Two-photon ${}^4A_2 \rightarrow {}^4T_2$ Spectrum of Mn^{4+} in the Cubic and Trigonal Sites of Cs_2MF_6 , $M = Si, Ge, Ti$. *Chem. Phys. Lett.* **1989**, *157*, 78–82.
- (39) Hasan, Z.; Manson, N. B. Electron-Vibration Effects in $Cs_2SiF_6:Mn^{4+}$. *Mol. Phys.* **1980**, *40*, 1227–1248.
- (40) Shannon, R. T. Revised Effective Ionic Radii and Systematic Studies of Interatomic Distances in Halides and Chalcogenides. *Acta Crystallogr., Sect. A: Cryst. Phys., Diffraction, Theor. Gen. Crystallogr.* **1976**, *32*, 751–767.
- (41) Arai, Y.; Adachi, S. Optical Transitions and Internal Vibronic Frequencies of MnF_6^{2-} Ions in Cs_2SiF_6 and Cs_2GeF_6 Red Phosphors. *J. Electrochem. Soc.* **2011**, *158* (6), J179–J183.
- (42) Barabash, S. V.; Blum, V.; Müller, S.; Zunger, A. Prediction of Unusual Stable Ordered structures of Au-Pd Alloys via a First-Principles Cluster Expansion. *Phys. Rev. B: Condens. Matter Mater. Phys.* **2006**, *74*, 035108.
- (43) Liao, J. H.; Zhao, Y. J.; Tang, J. J.; Yang, X. B.; Xu, H. High-Coverage Stable Structures of 3d Transition Metal Intercalated Bilayer Graphene. *Phys. Chem. Chem. Phys.* **2016**, *18*, 14244–14251.
- (44) Han, T.; Lang, T. C.; Wang, J.; Tu, M. J.; Peng, L. L. Large Micro-Sized $K_2TiF_6:Mn^{4+}$ Red phosphors Synthesised By a Simple Reduction Reaction for High Colour-rendering White light-Emitting Diodes. *RSC Adv.* **2015**, *5*, 100054–100059.
- (45) Suehiro, T.; Xie, R. J.; Hirosaki, N. Facile Synthesis of $(Sr,Ca)_2Si_3N_8:Eu^{2+}$ -Based Red-Emitting Phosphor for Solid-State Lighting. *Ind. Eng. Chem. Res.* **2013**, *52*, 7453–7456.
- (46) Suehiro, T.; Xie, R. J.; Hirosaki, N. Gas-Reduction–Nitridation Synthesis of $CaAlSiN_3:Eu^{2+}$ Fine Powder Phosphors for Solid-state Lighting. *Ind. Eng. Chem. Res.* **2014**, *53*, 2713–2717.
- (47) Bode, H.; Janssen, H.; Bandte, F. Über eine neue Darstellung des Kalium-hexafluoromanganats (IV). *Angew. Chem.* **1953**, *65*, 304–304.
- (48) Wang, L.; Wang, X. J.; Kohsei, T.; Yoshimura, K.; Izumi, M.; Hirosaki, N.; Xie, R. J. Highly Efficient Narrow-Band Green and Red Phosphors Enabling Wider Color-Gamut LED Backlight for More Brilliant Displays. *Opt. Express* **2015**, *23*, 28707–28717.
- (49) Kresse, G.; Furthmüller, J. Efficient Iterative Schemes for AB Initio Total-Energy Calculations Using a Plane-Wave Basis Set. *Phys. Rev. B: Condens. Matter Mater. Phys.* **1996**, *54*, 11169.
- (50) Kresse, G.; Joubert, D. From Ultrasoft Pseudopotentials to the Projector Augmented-Wave Method. *Phys. Rev. B: Condens. Matter Mater. Phys.* **1999**, *59*, 1758.
- (51) Li, Z. J.; Xu, W.; Yu, Y. Q.; Du, H. Y.; Zhen, K.; Wang, J.; Luo, L. B.; Qiu, H. L.; Yang, X. B. Monolayer Hexagonal Arsenene with Tunable Electronic Structures and Magnetic Properties via Impurity Doping. *J. Mater. Chem. C* **2016**, *4*, 362–370.
- (52) Perdew, J. P.; Burke, K.; Ernzerhof, M. Generalized Gradient Approximation Made Simple. *Phys. Rev. Lett.* **1996**, *77*, 3865.
- (53) Li, X. T.; Yang, X. B.; Zhao, Y. J. Geometrical Eigen-Subspace Framework Based Molecular Conformation Representation for Efficient Structure Recognition and Comparison. *J. Chem. Phys.* **2017**, *146*, 154108.
- (54) Liao, L. G.; Zhao, Y. J.; Cao, Z. X.; Yang, X. B. Minimum Vertex-Type Sequencing Indexing for Clusters on Square Lattice. *Sci. Rep.* **2017**, *7*, 392–397.